Hot-electron effect in spin relaxation of electrically injected electrons in intrinsic Germanium

2015 J. Phys.: Condens. Matter 27 255001

(http://iopscience.iop.org/0953-8984/27/25/255001)

IOP Publishing Journal of Physics: Condensed Matter
J. Phys.: Condens. Matter **27** (2015) 255001 (9pp) doi:10.1088/0953-8984/27/25/255001

Hot-electron effect in spin relaxation of electrically injected electrons in intrinsic Germanium

T Yu and M W Wu

Hefei National Laboratory for Physical Sciences at Microscale, Key Laboratory of Strongly-Coupled Quantum Matter Physics and Department of Physics, University of Science and Technology of China, Hefei, Anhui 230026, People's Republic of China

E-mail: mwwu@ustc.edu.cn.

Received 27 January 2015, revised 22 March 2015
Accepted for publication 26 March 2015
Published 28 May 2015

Abstract

The hot-electron effect in the spin relaxation of electrically injected electrons in intrinsic germanium is investigated by the kinetic spin Bloch equations both analytically and numerically. It is shown that in the weak-electric-field regime with $E \lesssim 0.5\,\mathrm{kV\,cm^{-1}}$, our calculations have reasonable agreement with the recent transport experiment in the hot-electron spin-injection configuration (2013 *Phys. Rev. Lett.* **111** 257204). We reveal that the spin relaxation is significantly enhanced at low temperature in the presence of weak electric field $E \lesssim 50\,\mathrm{V\,cm^{-1}}$, which originates from the obvious center-of-mass drift effect due to the weak electron–phonon interaction, whereas the hot-electron effect is demonstrated to be less important. This can explain the discrepancy between the experimental observation and the previous theoretical calculation (2012 *Phys. Rev.* B **86** 085202), which deviates from the experimental results by about two orders of magnitude at low temperature. It is further shown that in the strong-electric-field regime with $0.5 \lesssim E \lesssim 2\,\mathrm{kV\,cm^{-1}}$, the spin relaxation is enhanced due to the hot-electron effect, whereas the drift effect is demonstrated to be marginal. Finally, we find that when $1.4 \lesssim E \lesssim 2\,\mathrm{kV\,cm^{-1}}$ which lies in the strong-electric-field regime, a small fraction of electrons ($\lesssim$5%) can be driven from the L to Γ valley, and the spin relaxation rates are the same for the Γ and L valleys in the intrinsic sample without impurity. With the negligible influence of the spin dynamics in the Γ valley to the whole system, the spin dynamics in the L valley can be measured from the Γ valley by the standard direct optical transition method.

Keywords: spin relaxation, hot-electron effect, germanium

(Some figures may appear in colour only in the online journal)

1. Introduction

Recently, growing attention has been paid to the electron spin dynamics in germanium (Ge) due to the series of experiments including both the electrical [1–8] and optical measurements [9–14]. This experimental progress pave the way to utilizing the excellent property of Ge in the spintronic application [3, 5, 12, 15–22]. In Ge, due to the lack of the inversion asymmetry, the D'yakonov–Perel' (DP) mechanism [23] is absent. Moreover, the hyperfine interaction with the nuclei can be suppressed by the isotopic purification [24, 25]. Therefore, its spin relaxation time (SRT) is expected to be very long [3, 5, 12, 15–22]. Furthermore, in intrinsic Ge, the spin relaxation of electrically/optically injected electrons due to the electron-impurity scattering can be further suppressed [26]. Therefore, with the mature nanoelectronic fabrication technology of the Group IV semiconductors, intrinsic Ge is promising for the design and development of spintronic devices.

The electrical methods with the application of electric and/or magnetic fields include the three- or four-terminal Hanle configuration [1–7] and the ballistic spin-injection configuration [8]. In the three- or four-terminal Hanle

configuration, the typical SRTs measured are in the order of nanoseconds at low temperature and tens of picoseconds at high temperature [1–7]. In the ballistic spin-injection configuration, based on the magnetic-field-induced spin relaxation channel arising from the anisotropy of the g-factor of different L-valleys, Li *et al* have measured the SRT by means of the spin transport under a magnetic field in the order of 100 Gauss [8]. The SRT was measured to be in the order of several hundreds of nanoseconds at low temperature around 50 K [8]. Moreover, a sensitive electric field dependence at weak electric fields ($\lesssim$50 V cm^{-1}) was observed, which was speculated to be the hot-electron effect [8]. It is noted that the SRTs measured in the ballistic spin-injection configuration are one to two orders of magnitude larger than thoses from the three- or four-terminal Hanle configuration, which are typically carried out with metallic doping concentrations (above the metal-to-insulator transition). With the electrodes attached to the surface of the sample in the three- or four-terminal Hanle configuration, it was speculated that the presence of interfaces and surface roughness could have a great influence on the intrinsic spin relaxation [2–6, 27–30]. Besides, the presence of impurities in the tunnel barrier may also provide a possible explanation for the discrepancy [31–35].

For the optical measurements, with the optical injection, several methods have been developed and applied in Ge to determine the electron SRT [9–14]. Guite *et al* have developed a novel method based on the sensitively tuned radio-frequency coil to measure the temporal evolution of the magnetization arising from the optical-injected spin polarization in Ge directly under the magnetic field (up to 80 Gauss) [9]. The temperature dependence of the electron SRT was measured to decrease from ∼5 ns to ∼2 ns from 100 K to 180 K [9]. Furthermore, in the work of Lohrentz *et al* [14], by means of the resonant spin amplification method, the electron SRT exceeding 65 ns at 60 K was measured. Moreover, a peak for the SRT appeared in the temperature dependence, which was speculated to be the influence of the electron-impurity scattering. It is noted that the SRTs measured from the optical measurements [9, 14] are in the same order as those from the electric method in the spin-injection configuration [8].

Meanwhile, the theoretical studies for the electron spin dynamics in intrinsic Ge are in progress [19, 21, 22]. With the establishment of the electron–phonon interaction in the L-valley by the group-theory method, the SRT for the spin relaxation due to the electron–phonon scattering in the framework of the Elliott-Yafet (EY) mechanism [36, 37] has been calculated in the non-degenerate limit [19, 21]. It has been found that the main spin relaxation source in intrinsic Ge comes from the inter-L valley electron–phonon interaction [19, 21]. However, up to now, there still exists a marked discrepancy between the experimental observation and the theoretical calculation, especially at low temperature, at which the theoretical calculations are two to three orders of magnitude larger than the experimental observations [7–9, 14]. In the intrinsic sample, this was speculated to be the hot-electron effect in the transport experiment [8]. Therefore, a full investigation into the hot-electron effect in the spin relaxation is needed. Moreover, although the hot-electron effect has been well studied in the charge transport experiment in Ge [38, 39], its influence on the spin relaxation has not yet been revealed. In the charge transport experiment, it has been revealed that due to the weak electron–phonon interaction in Ge, the hot-electron effect can be easily achieved especially at low temperature [38, 39]. This feature indicates that the electric field can influence the behavior of spin relaxation easily due to the hot-electron effect.

In this work, we study the hot-electron effect in the spin relaxation in intrinsic Ge by the kinetic spin Bloch equations (KSBEs) [40–43] both analytically and numerically. When the electric field is weak, we compare our calculations with the recent transport experiment in the spin-injection configuration with a weak electric field [8]. Good agreements with the experimental data are obtained. It is found that due to the weak electron–phonon interaction [38, 39], at low temperature, even small electric fields ($\lesssim$50 V cm^{-1}) [8] can cause an obvious center-of-mass drift effect and hence significantly enhance the spin relaxation, whereas the hot-electron effect is demonstrated to be less important. When the electric field is relatively strong ($0.5 \lesssim E \lesssim 2$ kV cm^{-1}), we find that the SRT decreases with the increase of the electric field because of the increase of the hot-electron temperature and hence the enhancement of the electron–phonon scattering, whereas the drift effect is shown to be marginal. Finally, with the intra-Γ and intra-L-Γ electron–phonon interactions established by Liu *et al* [44], the influence of the Γ valley to the spin relaxation in the presence of the electric field is revealed. We find that within the strength of the electric fields under study, only a small fraction ($\lesssim$5%) of the electron can be driven from the L valley to the Γ valley. Therefore, the influence of the electron spin dynamics in the Γ valley to the whole system is marginal. We further reveal that in the intrinsic sample without impurity, the spin relaxation rates are the same for the Γ and L valleys, and hence the spin dynamics in the L valley can be measured from the Γ valley by the direct optical transition method.

This paper is organized as follows. In section 2, we set up the model and the KSBEs. In section 3, we present the main results obtained from the KSBEs both analytically and numerically. The calculated results under the weak electric field are compared with the experimental data (section 3.1). Then, under the relatively strong electric field, the influences of the hot-electron effect on the spin relaxation are presented (section 3.2). We summarize in section 4.

2. Model and KSBEs

We start our investigation of the electron spin relaxation in intrinsic Ge, where the four lowest valleys in the conduction band are located at the L points ($\frac{\pi}{a_0}(1,1,1)$, $\frac{\pi}{a_0}(-1,1,1)$, $\frac{\pi}{a_0}(1,-1,1)$ and $\frac{\pi}{a_0}(1,1,-1)$ with a_0 denoting the lattice constant). The Γ valley lies energetically above the L valley with $\Delta E_{\rm L}^{\Gamma} = 0.151$ eV [44, 45] and the X valley lies further above the Γ valley with $\Delta E_{\Gamma}^{\rm X} = 0.04$ eV [13]. In the spherically symmetric approximation, the electron effective masses of the L and Γ valleys are $m_{\rm L}^* = 0.22m_0$ ($m_l = 1.588m_0$, $m_t = 0.0815m_0$) [21] and $m_{\Gamma}^* = 0.038m_0$

($m_l = m_t = 0.038m_0$) [45] respectively, with m_0 representing the free electron mass. In our investigation with the electric field $E \lesssim 2\,\mathrm{kV\,cm^{-1}}$, we do not consider the X valley as the fraction of the electron in these valleys are negligible.

The KSBEs derived via the nonequilibrium Green function method with the generalized Kadanoff-Baym Ansatz read [40–43, 46]

$$\partial_t \rho_{\lambda\mathbf{k}_\lambda} = \partial_t \rho_{\lambda\mathbf{k}_\lambda}|_{\mathrm{drift}} + \partial_t \rho_{\lambda\mathbf{k}_\lambda}|_{\mathrm{scat}}, \tag{1}$$

in which $\rho_{\lambda\mathbf{k}_\lambda}$ is the density matrix of electrons with momentum $\mathbf{k}_\lambda$ in the λ valley. Here, $\mathbf{k}_\lambda$ is defined in reference to the valley center in the valley coordinate, whose $\hat{z}$-axis is along the valley axis [21, 44]. The diagonal term $\rho_{\lambda\mathbf{k}_\lambda,\sigma\sigma} \equiv f_{\lambda\mathbf{k}_\lambda,\sigma}$ ($\sigma = \pm 1/2$) describes the distribution of electrons in each spin band, and the off-diagonal term $\rho_{\lambda\mathbf{k}_\lambda,\frac{1}{2}-\frac{1}{2}} = \rho^*_{\lambda\mathbf{k}_\lambda,-\frac{1}{2}\frac{1}{2}}$ represents the coherence between the two spin bands.

In the KSBEs, the drift term is given by

$$\partial_t \rho_{\lambda\mathbf{k}_\lambda}|_{\mathrm{drift}} = -e\mathbf{E}\cdot\nabla_{\lambda\mathbf{k}_\lambda}\rho_{\lambda\mathbf{k}_\lambda}, \tag{2}$$

with $e < 0$. $\partial_t \rho_{\lambda\mathbf{k}_\lambda}|_{\mathrm{scat}}$ stands for the scattering term, which includes the electron–phonon (ep), electron-impurity (ei) and electron-electron (ee) Coulomb scatterings:

$$\partial_t \rho_{\lambda\mathbf{k}_\lambda}\big|_{\mathrm{scat}} = \partial_t \rho_{\lambda\mathbf{k}_\lambda}\big|_{\mathrm{ep}} + \partial_t \rho_{\lambda\mathbf{k}_\lambda}\big|_{\mathrm{ei}} + \partial_t \rho_{\lambda\mathbf{k}_\lambda}\big|_{\mathrm{ee}}. \tag{3}$$

Explicit forms of these scattering terms are shown in appendix A.

The initial conditions at time $t = 0$ are prepared as follows. We turn on the electric field at $t = -t_0$, where the system is in the equilibrium, and the density matrix are expressed as

$$f_{\lambda\mathbf{k}_\lambda,\sigma}(-t_0) = \left\{\exp[(\varepsilon^\lambda_{\mathbf{k}_\lambda} - \mu)/(k_\mathrm{B}T)] + 1\right\}^{-1}, \tag{4}$$

$$\rho_{\lambda\mathbf{k}_\lambda,\frac{1}{2}-\frac{1}{2}}(-t_0) = \rho^*_{\lambda\mathbf{k}_\lambda,-\frac{1}{2}\frac{1}{2}}(-t_0) = 0, \tag{5}$$

with μ being the chemical potential for the electron at temperature T. The system is driven to the steady state before $t = 0$. Then at time $t = 0$, the chemical potential is modified to obtain the spin-polarized state with the spin polarization $P_0 = (N_\uparrow - N_\downarrow)/(N_\uparrow + N_\downarrow)$. Here, $N_{\uparrow(\downarrow)} = \sum_{\lambda,\mathbf{k}_\lambda} f_{\lambda\mathbf{k}_\lambda,\uparrow(\downarrow)}$ is the electron density of the spin-up (-down) state. When $t \geqslant 0$, the system relaxes from the spin-polarized state with the spin polarization $P(t) = \sum_{\lambda\mathbf{k}_\lambda} \mathrm{Tr}[\rho_{\lambda\mathbf{k}_\lambda}(t)\sigma_z]/n_e$ solved by the KSBEs. Here, $n_e = \sum_{\lambda,\mathbf{k}_\lambda} \mathrm{Tr}[\rho_{\lambda\mathbf{k}_\lambda}(t)]$ is the electron density.

3. Results

3.1. Analytical results

Before performing the full numerical calculation by solving the KSBEs, we first investigate the spin relaxation analytically with the drift effect and the hot-electron effect explicitly included. It has been demonstrated that at a relatively high temperature, the dominant spin relaxation channel in Ge arises from the inter-L valley electron–phonon interaction, in which the momentum dependencies of the matrix elements for the electron–phonon interaction and the phonon energy are negligible [21].

For the electron–phonon interaction, the matrix elements can be generally constructed in this form [19, 21, 44],

$$M^\gamma_{\mathbf{k}_\lambda,\mathbf{k}'_{\lambda'}} = A^\gamma_{\mathbf{k}_\lambda,\mathbf{k}'_{\lambda'}}\hat{I} + \mathbf{B}^\gamma_{\mathbf{k}_\lambda,\mathbf{k}'_{\lambda'}}\cdot\boldsymbol{\sigma}, \tag{6}$$

including both the spin-conserving and spin-flip parts for the interaction of electrons with the γ-branch phonon, where $\hat{I}$ and $\boldsymbol{\sigma}$ are 2×2 unit and Pauli matrices. The SRT due to the inter-L valley electron–phonon interaction can be directly deduced from the scattering term (equation (A.1)) in the KSBEs ($\hbar \equiv 1$ throughout this paper) [19, 21]

$$\begin{aligned}\frac{1}{\tau_s^{\mathrm{ep}}} = {}& \frac{2\pi}{Vd}\sum_{\mathbf{k}_\lambda}\sum_{\mathbf{k}'_{\lambda'},\lambda\neq\lambda'}\sum_{\gamma,\pm}\delta(\pm\Omega^\gamma_{\mathbf{k}'_{\lambda'}-\mathbf{k}_\lambda} + \varepsilon_{\mathbf{k}'_{\lambda'}} - \varepsilon_{\mathbf{k}_\lambda}) \\ & \times \frac{1}{\Omega^\gamma_{\mathbf{k}'_{\lambda'}-\mathbf{k}_\lambda}} N^{\gamma,\pm}_{\mathbf{k}'_{\lambda'}-\mathbf{k}_\lambda}(|B^{\gamma,x}_{\mathbf{k}_\lambda,\mathbf{k}'_{\lambda'}}|^2 + |B^{\gamma,y}_{\mathbf{k}_\lambda,\mathbf{k}'_{\lambda'}}|^2) \\ & \times (f^d_{\mathbf{k}_\lambda\uparrow} - f^d_{\mathbf{k}_\lambda\downarrow})\left[\sum_{\mathbf{k}_\lambda}(f^d_{\mathbf{k}_\lambda\uparrow} - f^d_{\mathbf{k}_\lambda\downarrow})\right]^{-1},\end{aligned} \tag{7}$$

in which, V and d are the volume and density of the crystal, respectively; γ labels the associated phonon branches in the X point connecting the two L valleys, including X_{1a}, X_{1b}, X_{4a} and X_{4b} phonons [19, 21, 44]; $N^{\gamma,\pm}_{\mathbf{k}'_{\lambda'}-\mathbf{k}_\lambda} = N^\gamma_{\mathbf{k}'_{\lambda'}-\mathbf{k}_\lambda} + \frac{1}{2} \pm \frac{1}{2}$ and $N^\gamma_{\mathbf{k}'_{\lambda'}-\mathbf{k}_\lambda} = \left\{\exp[\Omega^\gamma_{\mathbf{k}'_{\lambda'}-\mathbf{k}_\lambda}/(k_\mathrm{B}T)] - 1\right\}^{-1}$ is the Bose distribution of phonons with energy $\Omega^\gamma_{\mathbf{k}'_{\lambda'}-\mathbf{k}_\lambda}$; $f^d_{\mathbf{k}_\lambda\sigma}$ is the drifted Fermi distribution function of the electron in the steady state, which reads as [47–49]

$$f^d_{\mathbf{k}_\lambda\sigma} = \left\{\exp\left[\frac{(\mathbf{k}_\lambda - m^*_\lambda\mathbf{v}_\lambda)^2}{2m^*_\lambda} - \mu_\sigma\right]/(k_\mathrm{B}T_e) + 1\right\}^{-1}, \tag{8}$$

with $\mathbf{v}_\lambda$ being the steady-state drift velocity of the λ valley and T_e standing for the hot-electron temperature. One notices that the drifted Fermi distribution function (equation (8)) is widely used in the treatment of nonlinear transport in semiconductors [47–49]. In equation (8), $\mathbf{v}_\lambda$ is numerically obtained from the steady-state value of $\mathbf{v}_\lambda(t) \equiv \sum_{\mathbf{k}_\lambda\sigma}[f_{\mathbf{k}_\lambda,\sigma}(t)\hbar\mathbf{k}_\lambda/m_\lambda]/\sum_{\mathbf{k}_\lambda\sigma} f_{\mathbf{k}_\lambda,\sigma}(t)$, and T_e is obtained by fitting the Boltzmann tail of the numerically calculated steady-state electron distribution of each valley from the KSBEs.

When the electric field is weak with the condition $\frac{1}{2}m^*_\mathrm{L}\mathbf{v}^2_\lambda \ll k_\mathrm{B}T_e$ or $\frac{1}{2}m^*_\mathrm{L}\mathbf{v}^2_\lambda\beta_e \ll 1$ [$\beta_e = 1/(k_\mathrm{B}T_e)$] satisfied, we expand the steady-state distribution function to the order of $\mathbf{v}^2_\lambda$. Accordingly, in the small spin polarization and non-degenerate limit, the SRT due to the inter-L valley electron–phonon interaction (equation (7)) can be obtained

$$\frac{1}{\tau_s^{\mathrm{ep}}} = \sum_\gamma \frac{1}{\tau_s^\gamma(\mathbf{v}_\lambda = 0)}\left[1 + F(\beta_e\Omega_\gamma)\beta_e m^*_\mathrm{L}\mathbf{v}^2_\lambda\right], \tag{9}$$

with

$$\begin{aligned}\frac{1}{\tau_s^\gamma(\mathbf{v}_\lambda = 0)} = {}& \frac{\sqrt{\beta_e}}{8d}\left(\frac{2m^*_\mathrm{L}}{\pi}\right)^{3/2} K_1\left(\frac{\beta_e\Omega_\gamma}{2}\right) \\ & \times \left(|B^{\gamma,x}|^2 + |B^{\gamma,y}|^2\right)\frac{A_\gamma}{\sinh(\beta\Omega_\gamma/2)}\cosh\left(\frac{\beta - \beta_e}{2}\Omega_\gamma\right)\end{aligned} \tag{10}$$

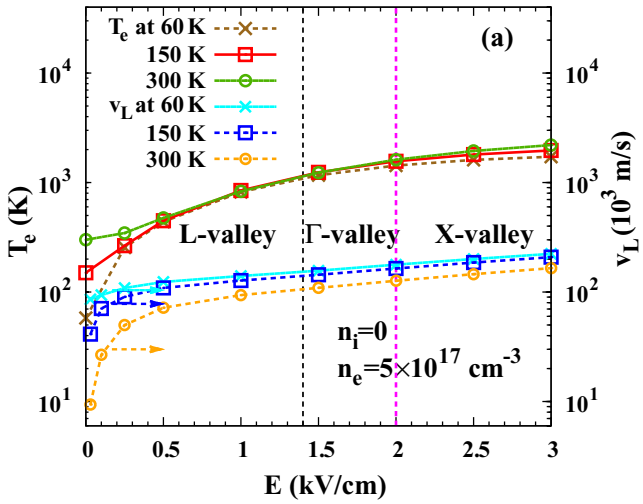

Figure 1. Electric field dependence of the hot-electron temperature and steady-state drift velocity (note the scale of both curves is on the right hand side of the frame) for electrons in the L valley at different temperatures (60, 150 and 300 K) with the electron density $n_e = 5 \times 10^{17}\,\mathrm{cm}^{-3}$. The pink (black) vertical dashed line at $E \approx 1.4\,\mathrm{kV\,cm}^{-1}$ ($E \approx 2\,\mathrm{kV\,cm}^{-1}$) corresponds to the boundary at which the Γ (X) valley becomes relevant for the spin relaxation.

and

$$F(x) = \frac{\sqrt{\pi}}{2x}\frac{U(-0.5,-2,x)}{K_1(x/2)}\exp(-x/2) - \frac{1}{2}. \qquad (11)$$

In equations (9) and (10), for the inter-L valley scattering with $|\mathbf{K}_{\mathrm{L}_i} - \mathbf{K}_{\mathrm{L}_j}| \gg |\mathbf{k}_\lambda|$ ($i \neq j$), the momentum dependencies of the matrix elements for the electron–phonon interaction and the phonon energy are negligible [21] and hence their labels of momentum are omitted. $\beta = 1/(k_{\mathrm{B}}T)$ with T being the lattice temperature. $\mathrm{A}_\gamma = 16$ ($\mathrm{A}_\gamma = 8$) for X_{1a} and X_{1b} (X_{4a} and X_{4b}) phonons [21]. $K_1(x/2)$ and $U(-0.5,-2,x)$ are the modified Bessel function of the second kind and Tricomi's confluent hypergeometric function, respectively.

It is noted that our results in equations (9) and (10) are 3/8 times of that in the work of Li *et al* (equation (10) in [21]) when $\beta = \beta_e$ and $\mathbf{v}_\lambda = 0$. However, by means of the same equation (equation (7)) here, the SRT due to the f-process of the electron–phonon scattering in Silicon (equation (18) in [18]) can be recovered. Moreover, our analytical results are further confirmed by the numerical ones as shown in the next section (refer to figure 1). Therefore, the results in the work of Li *et al* (equation (10) in [21]) underestimate the spin relaxation rate in intrinsic Ge, and should be corrected.

From the analytical results, it is seen that the spin relaxation rates are independent of the electron density in the non-degenerate regime. Moreover, the effect of the drift and hot-electron effects in the spin relaxation under the weak electric field can be obtained. First of all, it can be shown that the drift effect can enhance the spin relaxation with the factor $F(x)$ (equation (11)) always larger than zero. However, under the weak electric field, with $F(x)$ decreasing from 1/6 monotonically to 0 when x increases from 0, it shows that the influence of the drift effect due to the electric field to the spin relaxation is marginal when $F(x)\beta_e m_{\mathrm{L}}^* \mathbf{v}_\lambda^2 \ll 1$. In this situation, the electron SRT in the presence of the electric field can be approximately obtained from equation (10), and hence the hot-electron effect has a dominant influence on the spin relaxation. When the hot-electron temperature increases, $\sqrt{\beta_e}$ decreases slowly, $K_1(\beta_e\Omega_\gamma/2)$ increases rapidly and $\cosh[(\beta - \beta_e)\Omega_\gamma/2]$ increases slowly. Hence, the SRT decreases with the increase in the hot-electron temperature. It can also be obtained that when the lattice temperature increases, $[\sinh(\beta\Omega_\gamma/2)]^{-1}$ increases and $\cosh[(\beta - \beta_e)\Omega_\gamma/2]$ (when $\beta_e \lesssim \beta$) and $\sqrt{\beta_e}$ decrease slowly. Hence, the SRTs decreases with the increase in the lattice temperature [21].

Table 1. Parameters used in the computation.

m_{L}^*/m_0	0.22^a	$\Omega_{\mathrm{L}1}$ (meV)	29.3^c
m_Γ^*/m_0	0.038^b	$\Omega_{\mathrm{L}3}$ (meV)	7.2^c
$\Delta E_{\mathrm{L}}^\Gamma$ (eV)	$0.151^{b,c}$	$\Omega_{\mathrm{L}2'}$ (meV)	25.6^c
$\Delta E_\Gamma^{\mathrm{X}}$ (eV)	0.04^d	$\Omega_{\mathrm{L}3'}$ (meV)	35.8^c
$d(10^3\,\mathrm{kg\,cm}^{-3})$	5.323^e	$D_{\mathrm{X}1\mathrm{s}}$ (eV nm^{-1})	0.18^c
κ_0	16.0^f	$D_{\mathrm{X}4\mathrm{s}}$ (eV nm^{-1})	0.66^c
v_{LA} (m s^{-1})	4900^e	$D_{\mathrm{x}1\mathrm{m}}$ (eV nm^{-1})	6.56^c
v_{TA} (m s^{-1})	3500^e	$A_{\mathrm{L}2'}$ (eV nm^{-1})	18.21^c
$\Omega_{\mathrm{LO},\Gamma}$ (meV)	38.2^c	$B_{\mathrm{L}3'y}$ (eV nm^{-1})	$-0.35\,i^c$
$\Omega_{\mathrm{X}1}$ (meV)	28.4^c	P_0	$30\%^d$
$\Omega_{\mathrm{X}4}$ (meV)	33.3^c	t_0 (ps)	30
$\Omega_{\mathrm{X}3}$ (meV)	10.2^c		

[a] [21], [b] [45], [c] [44], [d] [13], [e] [19], [f] [53].

3.2. Numerical results

In this section, we present our results obtained by numerically solving the KSBEs following the scheme laid out in [50–52]. All parameters including the material parameters, band structure and phonon parameters used in our computation are listed in table 1. During the calculation, the impurity density n_i is set to be zero in the intrinsic sample. Furthermore, in the intrinsic sample, the electron can be injected by means of the electrical and optical methods [8–14, 19, 21, 22], whose density n_e varies from 10^{13} to $10^{17}\,\mathrm{cm}^{-3}$.

Before the full numerical investigation, we first present the electric field dependence of the hot-electron temperature and steady-state drift velocity when the electron density $n_e = 5 \times 10^{17}\,\mathrm{cm}^{-3}$. We find that the spin relaxation in intrinsic Ge in the presence of the electric field can be divided into three regimes according to the hot-electron temperature: (1) when $E \lesssim 1.4\,\mathrm{kV\,cm}^{-1}$, only the L valley is relevant for the spin relaxation; (2) when $1.4 \lesssim E \lesssim 2\,\mathrm{kV\,cm}^{-1}$, the Γ valley becomes relevant; (3) when $E \gtrsim 2\,\mathrm{kV\,cm}^{-1}$, the X valley becomes relevant. The boundaries between different regimes are shown in figure 1, where the electric field dependence of the hot-electron temperature for electrons in the L valley with $n_e = 5 \times 10^{17}\,\mathrm{cm}^{-3}$ at different temperatures ($T = 60$, 150 and 300 K) is presented (the steady-state drift velocity is also shown). It can be seen that both the hot-electron temperature and the steady-state drift velocity increase with increasing the electric field. For electrons with the Boltzmann distribution and marginal drift effect ($\frac{1}{2}m_{\mathrm{L}}^*\mathbf{v}_\lambda^2\beta_e \ll 1$), its average energy is estimated to be $\bar{E} = \frac{3}{2}k_{\mathrm{B}}T_e$. Accordingly, the hot-electron temperatures at which electrons can be driven to the Γ and X valleys efficiently are estimated to be $\Delta E_{\mathrm{L}}^\Gamma/(\frac{3}{2}k_{\mathrm{B}}) \approx 1200\,\mathrm{K}$

and $(\Delta E_{\mathrm{L}}^{\Gamma} + \Delta E_{\Gamma}^{\mathrm{X}})/(\frac{3}{2}k_{\mathrm{B}}) \approx 1500\,\mathrm{K}$, corresponding to $E \approx 1.4\,\mathrm{kV\,cm^{-1}}$ (shown as the black vertical dashed line) and $2\,\mathrm{kV\,cm^{-1}}$ (shown as the pink vertical dashed line) in figure 1, respectively. We emphasize that this division of the system is irrelevant to the electron density in the non-degenerate regime. We further perform the calculation with $n_e = 10^{13}\,\mathrm{cm^{-3}}$ with the Fermi temperature $T_{\mathrm{F}} \approx 1\,\mathrm{K}$, which are not shown in figure 1 for their coincidences with the ones with $n_e = 5 \times 10^{17}\,\mathrm{cm^{-3}}$ ($T_{\mathrm{F}} \approx 45\,\mathrm{K}$). In this work, we study the spin relaxation in the presence of the electric field E up to $2\,\mathrm{kV\,cm^{-1}}$ under which the L and Γ valleys are relevant.

In figure 1, some features should be further addressed. It is shown that when $E \lesssim 0.5\,\mathrm{kV\,cm^{-1}}$, with the increase of the electric field, the hot-electron temperature increases slowly, whereas the drift velocity increases rapidly (even when $E \lesssim 0.1\,\mathrm{kV\,cm^{-1}}$); when $0.5 \lesssim E \lesssim 3\,\mathrm{kV\,cm^{-1}}$, the hot-electron temperature increases, whereas the drift velocity becomes saturate. Specifically, when the electric field is extremely weak $E \lesssim 0.1\,\mathrm{kV\,cm^{-1}}$, the hot-electron temperature equals to the lattice one approximately at different temperatures (60, 150 and 300 K). These features are consistent with the experimental observations about the drift velocity [38, 39]. Accodingly, the electric field can be divided into weak- ($E \lesssim 0.5\,\mathrm{kV\,cm^{-1}}$) and strong-electric-field ($0.5 \lesssim E \lesssim 2\,\mathrm{kV\,cm^{-1}}$) regimes.

3.2.1. Spin relaxation under a weak electric field: comparison with experiments. As mentioned in the introduction, the experiments on the electron spin relaxation in intrinsic Ge have been carried out recently by several methods including both the electrical [1–8] and optical ones [9–14]. Up to now, there still exists a marked discrepancy between the experimental observations and the theoretical calculations in the intrinsic sample, especially at low temperature around 30 K [8–14, 19, 21, 22]. This motivates us to carry out the full calculations including the electron–phonon and electron-electron Coulomb scatterings in the presence of the electric field. In the works of Lohrentz *et al* [14] and Li *et al* [8], the electron density is in the order of $n_e = 10^{13}\,\mathrm{cm^{-3}}$[1]. Accordingly, when comparing with the experiments [8, 14], we choose the typical electron density to be $n_e = 10^{13}\,\mathrm{cm^{-3}}$ here, which lies in the non-degenerate regime. From equation (9), we emphasize that the chosen electron density does not influence the spin relaxation rates in the non-degenerate regime [21, 40]. Our calculation further shows that even the electron density is taken to be $n_e = 5 \times 10^{17}\,\mathrm{cm^{-3}}$ realized in the optical experiment [12], which lies in the crossover region of the non-degenerate and degenerate regimes at low temperature with $T_{\mathrm{F}} \approx 45\,\mathrm{K}$, the spin relaxation rates are marginally influenced. The results in the presence of the weak electric field ($E \lesssim 50\,\mathrm{V\,cm^{-1}}$) are summarized in figures 2(*a*) and (*b*).

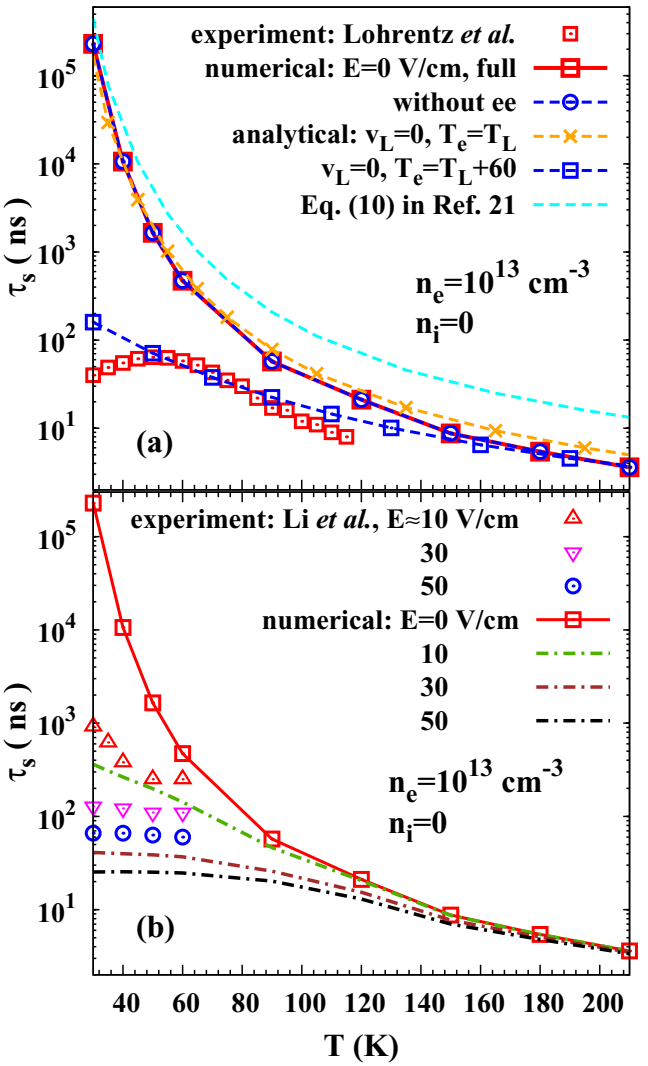

Figure 2. Electron SRTs in intrinsic Ge as a function of temperature. (*a*), experimental results: red open squares correspond to the experiment of Lohrentz *et al* ([14]). Numerical results: the red solid curve with squares (blue dashed curve with circles) corresponds to the numerical result with all the scatterings (without the electron-electron scattering). Analytical result: the orange dashed curve with crosses represents the analytical results calculated from equation (10) by setting $T_e = T$. The results calculated according to equation (10) in [21] by Li *et al* are plotted by the cyan dotted curve using parameters in work of Liu *et al* (simply 8/3 times of the orange dashed curve with crosses) [44]. (*b*), the experimental results of Li *et al* ([8]) are shown as red open upward triangles for $E \approx 10\,\mathrm{V\,cm^{-1}}$, pink open downward triangles for $E \approx 30\,\mathrm{V\,cm^{-1}}$, and blue open circles for $E \approx 50\,\mathrm{V\,cm^{-1}}$, respectively. Numerical results: when $n_i = 0$, the green, brown and black dot-dashed curves represent the SRTs calculated numerically with $E \approx$10, 30 and $50\,\mathrm{V\,cm^{-1}}$, respectively.

In figure 2(*a*), when electric field $E = 0$ and the impurity density $n_i = 0$, it can be seen that the SRTs with (the red solid curve with squares) and without (the blue dashed curve with circles) the electron–electron scattering coincide with each other. Therefore, the influence of the electron–electron

[1] In the optical experiment by Lohrenz *et al* [14], the photogenerated peak carrier density is stated to be $1.5 \times 10^{13}\,\mathrm{cm^{-3}}$ by the optical pulse in the nominally undoped sample. In the electrical experiment by Li *et al* [8], the samples are nominally undoped with the room-temperature resistivity > 40 Ω·cm. As the mobility limited by the electron–phonon scattering at 300 K is $2.8 \times 10^4\,\mathrm{cm^2/(V{\cdot}s)}$, and hence the corresponding electron density in the sample is fitted to be $< 5 \times 10^{12}\,\mathrm{cm^{-3}}$. However, this density is not necessarily the one participating in transport in the spin injection experiment by attaching magnetic contacts and the injected electron density is not reported in [8]. Therefore, in the numerical calculation, we choose the electron density to be $n_e = 10^{13}\,\mathrm{cm^{-3}}$, which is a little higher than $5 \times 10^{12}\,\mathrm{cm^{-3}}$.

scattering to the spin relaxation in the L valley is marginal. Moreover, the numerical results with all the scatterings (shown by the red solid curve with squares) are consistent with the analytical results calculated from equation (10) by setting T_e equal to the lattice temperature T_L (the orange dashed curve with crosses), in which only the inter-L valley scattering is included. This shows that the inter-L valley scattering is dominant for the spin relaxation [8]. The result calculated according to equation (10) using the parameters in the work of Liu *et al* [44] in [21] by Li *et al* is also plotted by the cyan dotted curve, showing a marked discrepancy compared with the full numerical result. Furthermore, it can be seen that the SRT decreases monotonically with the increase of the temperature. This is because with the increase of the temperature, the electron–phonon scattering is enhanced, which enhances the spin relaxation due to the EY mechanism [36, 37].

In figure 2(*a*), when the electric field is zero, we compare the temperature dependence of the electron SRTs obtained from our model with the optical experiments by Lohrentz *et al* (red open squares) [14]. One notices that these optical observations deviate by orders of magnitude from the calculations at $E = 0$. However, in figure 2(*a*), we show that when using an effective hot-electron temperature $T_e = (T_L + 60)$ K, the analytical results (green dashed curve with squares) are comparable with the experimental ones especially at $T \gtrsim 50$ K. Accordingly, this provides a possible explanation for the enhancement of the spin relaxation in the optical experiment [14]. In the optical experiments, the electrons are first optically injected to the Γ valley, which are then scattered to the L and X valleys through the inter-valley electron–phonon scattering [9–14]. Accordingly, with the weak intra-valley electron–phonon scattering [38, 39, 44], the cooling process is suppressed, and hence the hot-electron effect can arise easily [13]. Therefore, the enhancement of the spin relaxation in the optical experiments may arise from the hot-electron effect, which has been discussed in GaAs [50, 54, 55].

When a weak electric field ($\lesssim$50 V cm^{-1}) is applied, as shown in figure 2(*b*), we further compare our calculations with Li *et al* (the red open upward triangles for $E \approx 10$ V cm^{-1}, pink open downward triangles for 30 V cm^{-1}, and the blue open circles for 50 V cm^{-1}) [8]. In the experiment of Li *et al* [8], the samples are nominally undoped. Therefore, we perform the calculation with the impurity density $n_i = 0$. It is shown that the numerical results (the green, brown and black dot-dashed curves represent the SRTs calculated numerically with $E \approx 10$, 30 and 50 V cm^{-1}, respectively) are comparable with the experimental values, with the theoretical results being 1/3 to 1/2 of the experimental ones. Moreover, we further find that with the weak electric field ($E \lesssim 50$ V cm^{-1}), the electron temperature equals to the lattice one approximately, i.e. $T_e \approx T$, whereas $\frac{1}{2}\beta_e m_L^* \mathbf{v}_L^2 \approx 2.4$ at 30 K and $\frac{1}{2}\beta_e m_L^* \mathbf{v}_L^2 \gtrsim 1$ between 40 and 60 K when $E \approx 50$ V cm^{-1}. This shows that the hot-electron effect for the system in the presence of the weak electric field at low temperature is marginal, whereas the drift effect is obvious. Therefore, this significant enhancement of the spin relaxation in the presence of the weak electric field at low temperature arises from the drift effect rather than the hot-electron effect.

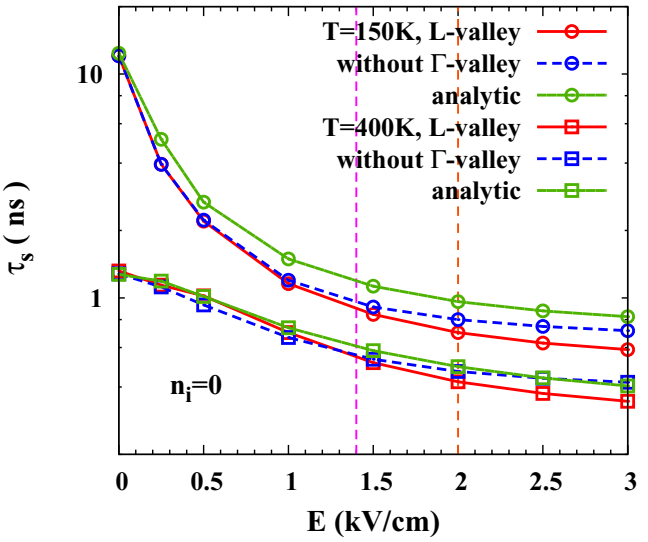

Figure 3. Electric field dependence of the electron SRTs in the L and Γ valleys in the impurity-free situation at 150 and 400 K, respectively. The analytical results, obtained from equations (9)–(11) with the hot-electron temperature and the steady-state drift velocity numerically calculated by the KSBEs, are shown by the green solid curve.

The enhancement of the spin relaxation due to the drift effect can be understood as follows. It has been addressed that the phonon-induced intervalley scattering between the L-valleys is the dominant spin-flip mechanism [8]. At low temperature, only phonon emission is feasible (involved phonon energy is about 30 meV) [21, 44], which needs the electron in the initial state to be 30 meV or more above the conduction-band edge. The drift effect can shift the electron distribution and hence increase the population of electrons with energies more than 30 meV needed to ignite the intervalley process. Accordingly, due to the drift effect, the inter-L valley spin–flip scattering is enhanced and hence the spin relaxation.

3.2.2. Hot-electron effect on the spin relaxation under a relatively strong electric field. In the presence of a relatively strong electric field ($0.5 \lesssim E \lesssim 3$ kV cm^{-1}), we first study the electric field dependence of the electron spin relaxation in Ge at different temperatures $T = 150$ and 400 K both numerically and analytically. In this subsection, in order to study the influence of the Γ valley on the spin relaxation, the electron density is set to be 5×10^{17} cm^{-3} [13], with more electrons driven to the Γ valley compared to the case with low electron density. In figure 3, the SRTs for the electrons in the L valley with (the red solid curves) and without the Γ valley (the dashed blue curves) are plotted against the electric field, which is extended to 3 kV cm^{-1}, in the impurity-free situation.

In figure 3, it can be seen that for both temperatures $T = 150$ and 400 K, the SRTs in the L valley (the red solid curves) decrease monotonically with the increase of the electric field. It is noted that in figure 1, we have presented the electric field dependencies of the hot-electron temperature and the steady-state drift velocity, which increase with the increasing electric field. From the analytical results in section 3.1, both the drift and hot-electron effects can enhance the spin relaxation.

Their contribution to the spin relaxation can be distinguished by using equations (9)–(11). With the numerical values of the hot-electron temperature and the steady-state drift velocity (figure 1), the analytical results with (the green solid curves) and without (by setting $\mathbf{v}_\lambda = 0$) the drift effect are calculated. We find that the two curves coincide with each other at both 150 and 400 K, which are both consistent with the numerical ones. Therefore, the influence of the drift effect to the spin relaxation at high temperature ($T \gtrsim 150$ K) is marginal. One concludes that the enhancement of the spin relaxation mainly originates from the hot-electron effect, where the increase in the hot-electron temperature enhances the electron–phonon interaction.

It has also been shown in figure 1 that at a relatively large electric field, the Γ ($E \gtrsim 1.4\,\mathrm{kV\,cm^{-1}}$) and X valleys ($E \gtrsim 2\,\mathrm{kV\,cm^{-1}}$) become relevant. Therefore, in our study, we include the Γ valley explicitly, and reveal its influence to the spin relaxation. It is shown in figure 3 that at both 150 and 400 K, the SRTs in the L valley with (the red solid curves) and without (the blue dashed curves) the Γ valley are almost the same, especially at a low electric field. This is because in the range of the electric field, the fractions of the electrons driven from the L to Γ valley are small (≲5%), and hence the Γ valley plays a marginal role in the spin relaxation of the whole system. Moreover, the numerical results show that the SRTs in the L and Γ (not shown in figure 3) valleys are almost the same. This arises from the strong inter-L-Γ valley electron–phonon interaction and hence the frequent exchange of electrons between the L and Γ valleys [51, 52]. Accordingly, the spin dynamics in the L valley in the presence of the electric field in the impurity-free situation can be measured from the Γ valley by the standard optical method [56–60]. It is noted that notwithstanding the fact that the calculated electric field is extended up to $3\,\mathrm{kV\,cm^{-1}}$ where the X valley becomes relevant, luckily the population of the electrons in that valley is still negligible. Therefore, the X valley has a marginal influence on the spin relaxation in the L valley we calculate above. One expects that with the electric field further increasing, the spin relaxation may be significantly enhanced at the X valleys once the electrons populate the spin hot spots (where the spin mixing is large) [61, 62].

4. Summary

In summary, we have investigated the hot-electron effect in the spin relaxation of electrically injected electrons in intrinsic Ge by the KSBEs both analytically and numerically [40]. We first compare our calculations with the recent transport experiment by Li *et al* [8] in the spin-injection configuration when the electric field is weak (≲$50\,\mathrm{V\,cm^{-1}}$). Our calculations agree with the experimental data fairly well, and hence can explain the marked discrepancy between the experiment of Li *et al* [8] and the previous theoretical calculations [7–9, 14]. It is revealed that at low temperature, even small electric fields (≲$50\,\mathrm{V\,cm^{-1}}$) [8] can cause an obvious center-of-mass drift effect due to the weak electron–phonon interaction in Ge [38, 39]. This can significantly enhance the spin relaxation, whereas the hot-electron effect is demonstrated to be less important.

We then study the spin relaxation when the electric field is relatively strong ($0.5 \lesssim E \lesssim 2\,\mathrm{kV\,cm^{-1}}$), under which the Γ valley becomes relevant. The electric field dependence of the spin relaxation is studied. We find that the SRT decreases with the increase in the electric field. This is because with the increase of the electric field, the hot-electron temperature increases, and hence the electron–phonon scattering is enhanced. Therefore, in the presence of the relatively strong electric field, the hot-electron effect has a marked influence on the spin relaxation, whereas the drift effect is shown to be marginal.

Finally, we further study the influence of the Γ valley on the spin relaxation in the presence of the electric field. We find that within the strength of the electric fields under study ($E \lesssim 2\,\mathrm{kV\,cm^{-1}}$), only a small fraction (≲5%) of the electron can be driven from the L valley to the Γ valley. Therefore, the influence of the electron spin dynamics in the Γ valley to the whole system is marginal. Nevertheless, we find that in the impurity-free situation, the spin relaxation rates are the same for the Γ and L valleys, and hence the spin dynamics in the L valley can be measured from the Γ valley by the standard optical methods.

Acknowledgments

This work was supported by the National Natural Science Foundation of China under Grant No. 11334014 and 61411136001, the National Basic Research Program of China under Grant No. 2012CB922002, and the Strategic Priority Research Program of the Chinese Academy of Sciences under Grant No. XDB01000000. One of the authors (TY) would like to thank M Q Weng for his suggestion on analytical derivation.

Appendix A. Scattering terms of the KSBEs

The scattering terms for the electron–phonon, electron-impurity and electron–electron scatterings are shown as,

$$\partial_t \rho_{\lambda\mathbf{k}_\lambda}\big|_{\mathrm{ep}} = -\pi \sum_{\lambda',\mathbf{k}'_{\lambda'},\pm} \sum_{\gamma} \delta(\pm\Omega^{\gamma}_{\mathbf{k}'_{\lambda'}-\mathbf{k}_\lambda} + \varepsilon^{\lambda'}_{\mathbf{k}'_{\lambda'}} - \varepsilon^{\lambda}_{\mathbf{k}_\lambda}) \times \Big(N^{\gamma,\pm}_{\mathbf{k}'_{\lambda'}-\mathbf{k}_\lambda} M^{\gamma}_{\mathbf{k}_\lambda,\mathbf{k}'_{\lambda'}} \rho^{>}_{\lambda'\mathbf{k}'_{\lambda'}} M^{\gamma}_{\mathbf{k}'_{\lambda'},\mathbf{k}_\lambda} \rho^{<}_{\lambda\mathbf{k}_\lambda} - N^{\gamma,\mp}_{\mathbf{k}'_{\lambda'}-\mathbf{k}_\lambda} \times M^{\gamma}_{\mathbf{k}_\lambda,\mathbf{k}'_{\lambda'}} \rho^{<}_{\lambda'\mathbf{k}'_{\lambda'}} M^{\gamma}_{\mathbf{k}'_{\lambda'},\mathbf{k}_\lambda} \rho^{>}_{\lambda\mathbf{k}_\lambda} \Big) + \mathrm{H.c.}; \tag{A.1}$$

$$\partial_t \rho_{\lambda\mathbf{k}_\lambda}|_{\mathrm{ei}} = -\pi n_i Z_i^2 \sum_{\mathbf{k}'_\lambda} V^2_{\mathbf{k}_\lambda-\mathbf{k}'_\lambda} (\hat{\Lambda}_{\lambda\mathbf{k}_\lambda,\lambda\mathbf{k}'_\lambda} \rho^{>}_{\lambda\mathbf{k}'_\lambda} \hat{\Lambda}_{\lambda\mathbf{k}'_\lambda,\lambda\mathbf{k}_\lambda} \rho^{<}_{\lambda\mathbf{k}_\lambda} - \hat{\Lambda}_{\lambda\mathbf{k}_\lambda,\lambda\mathbf{k}'_\lambda} \rho^{<}_{\lambda\mathbf{k}'_\lambda} \hat{\Lambda}_{\lambda\mathbf{k}'_\lambda,\lambda\mathbf{k}_\lambda} \rho^{>}_{\lambda\mathbf{k}_\lambda}) \delta(\varepsilon^{\lambda}_{\mathbf{k}'_\lambda} - \varepsilon^{\lambda}_{\mathbf{k}_\lambda}) + \mathrm{H.c.}; \tag{A.2}$$

$$\partial_t \rho_{\lambda\mathbf{k}_\lambda}\big|_{\mathrm{ee}} = -\pi \sum_{\lambda',\mathbf{k}'_\lambda,\mathbf{k}''_{\lambda'}} V^2_{\mathbf{k}_\lambda-\mathbf{k}'_\lambda} \delta(\varepsilon^{\lambda}_{\mathbf{k}'_\lambda} - \varepsilon^{\lambda}_{\mathbf{k}_\lambda} + \varepsilon^{\lambda'}_{\mathbf{k}''_{\lambda'}} - \varepsilon^{\lambda'}_{\mathbf{k}''_{\lambda'}-\mathbf{k}_\lambda+\mathbf{k}'_\lambda}) \times \Big\{ \hat{\Lambda}_{\lambda\mathbf{k}_\lambda,\lambda\mathbf{k}'_\lambda} \rho^{>}_{\lambda\mathbf{k}'_\lambda} \hat{\Lambda}_{\lambda\mathbf{k}'_\lambda,\lambda\mathbf{k}_\lambda} \rho^{<}_{\lambda\mathbf{k}_\lambda} \times \mathrm{Tr}\Big[\hat{\Lambda}_{\lambda'\mathbf{k}''_{\lambda'},\lambda'(\mathbf{k}''_{\lambda'}-\mathbf{k}_\lambda+\mathbf{k}'_\lambda)} \rho^{<}_{\lambda'(\mathbf{k}''_{\lambda'}-\mathbf{k}_\lambda+\mathbf{k}'_\lambda)} \hat{\Lambda}_{\lambda'(\mathbf{k}''_{\lambda'}-\mathbf{k}_\lambda+\mathbf{k}'_\lambda),\lambda'\mathbf{k}''_{\lambda'}} \rho^{>}_{\lambda'\mathbf{k}''_{\lambda'}} \Big]$$

$$- \hat{\Lambda}_{\lambda\mathbf{k}_\lambda,\lambda\mathbf{k}'_\lambda}\rho^{<}_{\lambda\mathbf{k}'_\lambda}\hat{\Lambda}_{\lambda\mathbf{k}'_\lambda,\lambda\mathbf{k}_\lambda}\rho^{>}_{\lambda\mathbf{k}_\lambda}$$
$$\times \mathrm{Tr}\left[\hat{\Lambda}_{\lambda'\mathbf{k}''_{\lambda'},\lambda'(\mathbf{k}''_{\lambda'}-\mathbf{k}_\lambda+\mathbf{k}'_\lambda)}\rho^{>}_{\lambda'(\mathbf{k}''_{\lambda'}-\mathbf{k}_\lambda+\mathbf{k}'_\lambda)}\hat{\Lambda}_{\lambda'(\mathbf{k}''_{\lambda'}-\mathbf{k}_\lambda+\mathbf{k}'_\lambda),\lambda'\mathbf{k}''_{\lambda'}}\rho^{<}_{\lambda'\mathbf{k}''_{\lambda'}}\right]\Bigg\}$$
$$+ \text{H.c.}. \tag{A.3}$$

Here, $\rho^{<}_{\mathbf{k}} = \rho_{\mathbf{k}}$ and $\rho^{>}_{\mathbf{k}} = 1 - \rho_{\mathbf{k}}$. $\varepsilon^{\mathrm{L}_i}_{\mathbf{k}_{\mathrm{L}_i}} = k^2_{\mathrm{L}_i}/(2m^*_{\mathrm{L}})$ and $\varepsilon^{\Gamma}_{\mathbf{k}_\Gamma} = k^2_\Gamma/(2m^*_\Gamma) + \Delta E^\Gamma_{\mathrm{L}}$. In equation (A.1), for the intra-Γ valley electron–phonon scattering ($\lambda = \lambda' = \Gamma$), the phonon branches include TA_1, TA_2, LA, TO_1, TO_2, and LO phonons, where the electron–phonon scattering with the $\mathbf{k}^0$-order is forbidden (for the spin-conserving (spin–flip) scattering, the matrix elements are proportional to $\mathbf{k}$ ($\mathbf{k}^3$)) [44]. For the intra-L valley scattering ($\lambda = \lambda' = \mathrm{L}$), the phonon branches include TO_1, TO_2, and LO phonons, and especially for the spin–flip scattering, the matrix elements are proportional to $\mathbf{k}^3$, which are neglected in our study when the inter-L valley scattering is dominant for spin relaxation [21, 44]. For the inter-Γ-L valley scattering, the phonon branches include L_1, L_3, $\mathrm{L}_{2'}$, and $\mathrm{L}_{3'}$ phonons, where the electron–phonon interactions with $\mathbf{k}^0$-order exist for both the spin-conserving and spin–flip scatterings [44]. For the inter-L valley electron–phonon scattering, the phonon branches include X_1 and X_4 phonons, where the electron–phonon interactions with $\mathbf{k}^0$-order also exist for both the spin-conserving and spin–flip scatterings [21, 44] and especially we add the electron–phonon scattering with the $\mathbf{k}$-order [44].

In equations (A.2) and (A.3), n_i is the impurity density and $Z_i = 1$ is the charge number of the impurity; $V_{\mathbf{q}}$ is the screened Coulomb potential under the random phase approximation [40, 50–52]. The spin mixing $\hat{\Lambda}_{\lambda\mathbf{k}_\lambda,\lambda'\mathbf{k}'_{\lambda'}} = \hat{I} - \frac{1}{2}\left[S^{(1)}_{\lambda\mathbf{k}_\lambda}S^{(1)\dagger}_{\lambda\mathbf{k}_\lambda} - 2S^{(1)}_{\lambda\mathbf{k}_\lambda}S^{(1)\dagger}_{\lambda'\mathbf{k}'_{\lambda'}} + S^{(1)}_{\lambda'\mathbf{k}'_{\lambda'}}S^{(1)\dagger}_{\lambda'\mathbf{k}'_{\lambda'}}\right]$. The matrix $S^{(1)}_{\lambda'\mathbf{k}'_{\lambda'}}$ for the Γ and L valleys can be found in the 14×14 $\mathbf{k}\cdot\mathbf{p}$ Hamiltonian [45] and 16×16 one, [44] whose explicit forms are shown as follows. For the Γ valley,

$$S^{(1)}_{\Gamma\mathbf{k}_\Gamma} = \tag{A.4}$$
$$\begin{pmatrix} \frac{1}{\sqrt{2}}\frac{P^+}{E_g} & -\sqrt{\frac{2}{3}}\frac{P^z}{E_g} & -\frac{1}{\sqrt{6}}\frac{P^-}{E_g} & 0 & -\frac{1}{\sqrt{3}}\frac{P^z}{E_g+\Delta} & -\frac{1}{\sqrt{3}}\frac{P^-}{E_g+\Delta} \\ 0 & \frac{1}{\sqrt{6}}\frac{P^+}{E_g} & -\sqrt{\frac{2}{3}}\frac{P^z}{E_g} & -\frac{1}{\sqrt{2}}\frac{P^-}{E_g} & -\frac{1}{\sqrt{3}}\frac{P^+}{E_g+\Delta} & \frac{1}{\sqrt{3}}\frac{P^z}{E_g+\Delta} \end{pmatrix},$$

where $P^z = Pk_z$, $P^\pm = Pk_\pm = P(k_x \pm k_y)$ with $E_P = (2/m_0)P^2 = 26.3\,\mathrm{eV}$, $E_g = 0.898\,\mathrm{eV}$ and $\Delta = 0.297\,\mathrm{eV}$ [45]. For the L valley,

$$S^{(1)}_{\mathrm{L}\mathbf{k}_\mathrm{L}} = \left(S^{\mathrm{left}}_{\mathrm{L}\mathbf{k}_\mathrm{L}}, S^{\mathrm{right}}_{\mathrm{L}\mathbf{k}_\mathrm{L}}\right), \tag{A.5}$$

where

$$S^{\mathrm{left}}_{\mathrm{L}\mathbf{k}_\mathrm{L}} = \begin{pmatrix} \frac{\alpha_4 k_-}{E_{c1}-E_{c6}} & -\frac{P_4 k_z}{E_{c1}-E_{c6}} & \frac{\sqrt{2}(P_3-\alpha_3)k_-}{E_{c1}-E_{c5}} & \frac{2\sqrt{2}\alpha_3 k_z}{E_{c1}-E_{c5}} \\ -\frac{P_4 k_z}{E_{c1}-E_{c6}} & -\frac{\alpha_4 k_+}{E_{c1}-E_{c6}} & \frac{2\sqrt{2}\alpha_3 k_z}{E_{c1}-E_{c5}} & \frac{\sqrt{2}(\alpha_3-P_3)k_+}{E_{c1}-E_{c5}} \\ -\frac{(P_3+\alpha_3)k_+}{E_{c1}-E_{c4}} & \frac{(P_3+\alpha_3)k_+}{E_{c1}-E_{c4}} & & \\ -\frac{(P_3+\alpha_3)k_-}{E_{c1}-E_{c4}} & -\frac{(P_3+\alpha_3)k_-}{E_{c1}-E_{c4}} & & \end{pmatrix}, \tag{A.6}$$

and

$$S^{\mathrm{right}}_{\mathrm{L}\mathbf{k}_\mathrm{L}} = \begin{pmatrix} -\frac{\Delta_2}{E_{c1}-E_{c2}} & 0 & -\frac{(P_1+\alpha_1)k_+}{E_{c1}-E_{v1}} & \frac{(P_1+\alpha_1)k_+}{E_{c1}-E_{v1}} \\ 0 & -\frac{\Delta_2}{E_{c1}-E_{c2}} & \frac{(P_1+\alpha_1)k_-}{E_{c1}-E_{v1}} & \frac{(P_1+\alpha_1)k_-}{E_{c1}-E_{v1}} \\ -\frac{2\sqrt{2}\alpha_1 k_z}{E_{c1}-E_{v2}} & \frac{\sqrt{2}(2\alpha_1-P_1)k_-}{E_{c1}-E_{v2}} & & \\ \frac{\sqrt{2}(P_1-2\alpha_1)k_+}{E_{c1}-E_{v2}} & -\frac{2\sqrt{2}\alpha_1 k_z}{E_{c1}-E_{v2}} & & \end{pmatrix}. \tag{A.7}$$

All the parameters in equations (A.6) and (A.7) are listed in table 1 of [44].

References

[1] Shen C *et al* 2010 *Appl. Phys. Lett.* **97** 162104
[2] Saito H, Watanabe S, Mineno Y, Sharma S, Jansen R, Yuasa S and Ando K 2011 *Solid State Commun.* **151** 1159
[3] Zhou Y, Han W, Chang L T, Xiu F, Wang M, Oehme M, Fischer I A, Schulze J, Kawakami R K and Wang K L 2011 *Phys. Rev.* B **84** 125323
[4] Jeon K R, Min B C, Jo Y H, Lee H S, Shin I J, Park C Y, Park S Y and Shin S C 2011 *Phys. Rev.* B **84** 165315
[5] Jain A *et al* 2011 *Appl. Phys. Lett.* **99** 162102
[6] Kasahara K, Baba Y, Yamane K, Ando Y, Yamada S, Hoshi Y, Sawano K, Miyao M and Hamaya K 2012 *J. Appl. Phys.* **111** 07C503
[7] Chang L T, Han W, Zhou Y, Tang J, Fischer I A, Oehme M, Schulze J, Kawakami R K and Wang K L 2013 *Semicond. Sci. Technol.* **28** 015018
[8] Li P, Li J, Qing L, Dery H and Appelbaum I 2013 *Phys. Rev. Lett.* **111** 257204
[9] Guite C and Venkataraman V 2011 *Phys. Rev. Lett.* **107** 166603
Guite C and Venkataraman V 2012 *Appl. Phys. Lett.* **101** 252404
[10] Hautmann C, Surrer B and Betz M 2011 *Phys. Rev.* B **83** 161203
[11] Hautmann C and Betz M 2012 *Phys. Rev.* B **85** 121203
[12] Pezzoli F *et al* 2012 *Phys. Rev. Lett.* **108** 156603
[13] Pezzoli F, Qing L, Giorgioni A, Isella G, Grilli E, Guzzi M and Dery H 2013 *Phys. Rev.* B **88** 045204
[14] Lohrenz J, Paschen T and Betz M 2014 *Phys. Rev.* B **89** 121201
[15] Loren E J, Ruzicka B A, Werake L K, Zhao H, van Driel H M and Smirl A L 2009 *Appl. Phys. Lett.* **95** 092107
[16] Rioux J and Sipe J E 2010 *Phys. Rev.* B **81** 155215
[17] Loren E J, Rioux J, Lange C, Sipe J E, van Driel H M and Smirl A L 2011 *Phys. Rev.* B **84** 214307
[18] Li P and Dery H 2011 *Phys. Rev. Lett.* **107** 107203
[19] Tang J M, Collins B T and Flatté M E 2012 *Phys. Rev.* B **85** 045202
[20] Jain A *et al* M 2012 *Appl. Phys. Lett.* **101** 022402
[21] Li P, Song Y and Dery H 2012 *Phys. Rev.* B **86** 085202
[22] Li P, Trivedi D and Dery H 2013 *Phys. Rev.* B **87** 115203
[23] D'yakonov M I and Perel' V I 1971 *Zh. Eksp. Teor. Fiz.* **60** 1954
D'yakonov M I and Perel' V I 1971 *Sov. Phys.—JETP* **33** 1053
[24] Kane B E 1998 *Nature* **393** 133
[25] Fodor P S and Levy J 2006 *J. Phys.: Condens. Matter* **18** S745
[26] Song Y, Chalaev O and Dery H 2014 *Phys. Rev. Lett.* **113** 167201
[27] Tran M, Jaffrés H, Deranlot C, George J M, Fert A, Miard A and Lemaître A 2009 *Phys. Rev. Lett.* **102** 036601
[28] Dash S P, Sharma S, Le J C, Peiro J, Jaffrés H, George J M, Lemaître A and Jansen R 2011 *Phys. Rev.* B **84** 054410
[29] Li C H, van't Erve O M J and Jonker B T 2011 *Nat. Commun.* **2** 245
[30] Dash S P, Sharma S, Patel R S, de Jong M P and Jansen R 2009 *Nature* **462** 491
[31] Song Y and Dery H 2014 *Phys. Rev. Lett.* **113** 047205
[32] Txoperena O, Song Y, Qing L, Gobbi M, Hueso L E, Dery H and Casanova F 2014 *Phys. Rev. Lett.* **113** 146601
[33] Tinkey H N, Li P and Appelbaum I 2014 *Appl. Phys. Lett.* **104** 232410
[34] Swartz A G, Harashima S, Xie Y, Lu D, Kim B, Bell C, Hikita Y and Hwang H Y 2014 *Appl. Phys. Lett.* **105** 032406
[35] Yue Z and Raikh M E 2015 arXiv: 1502.00350
[36] Yafet Y 1952 *Phys. Rev.* **85** 478
[37] Elliott R J 1954 *Phys. Rev.* **96** 266
[38] McGroddy J C, Nathan M I and Smith J E Jr 1969 *IBM J. Res. DeV.* **13** 543

[39] Jacoboni C, Nava F, Canali C and Ottaviani G 1981 *Phys. Rev.* B **24** 1014
[40] Wu M W, Jiang J H and Weng M Q 2010 *Phys. Rep.* **493** 61
[41] Wu M W and Metiu H 2000 *Phys. Rev.* B **61** 2945
[42] Wu M W and Ning C Z 2000 *Eur. Phys. J.* B **18** 373
Wu M W 2001 *J. Phys. Soc. Japan* **70** 2195
[43] Weng M Q and Wu M W 2003 *Phys. Rev.* B **68** 075312
[44] Liu Z, Nestoklon M O, Cheng J L, Ivchenko E L and Wu M W 2013 *Fiz. Tverd. Tela* **55** 1510
Liu Z, Nestoklon M O, Cheng J L, Ivchenko E L and Wu M W 2013 *Fiz. Tverd. Tela* 2013 *Phys. Solid State* **55** 1619
[45] Ridene S, Boujdaria K, Bouchriha H and Fishman G 2001 *Phys. Rev.* B **64** 085329
[46] Haug H and Jauho A P 1996 *Quantum Kinetics in Transport and Optics of Semiconductors* (Berlin: Springer)
[47] Lifshitz E M and Pitaevskii L P 1981 *Physical Kinetics* (Oxford: Pergamon)
Uhlenbeck G E, Ford G W and Montroll E W 1963 *Lectures in Statistical Mechanics* (Providence, RI: American Mathematical Society) chapter 4
Gantmakher V F and Levinson Y B 1987 *Carrier Scattering in Metals and Semiconductors* (Amsterdam: North-Holland) chapter 6
[48] Fröhlich H and Paranjape B V 1956 *Proc. R. Soc. Lond.* B **69** 21
Hess K 1980 *Physics of Nonlinear Transport in Semiconductors* ed D K Ferry *et al* (New York: Plenum) p 1
Ferry D K 1980 *Physics of Nonlinear Transport in Semicon ductors* ed D K Ferry *et al* (New York: Plenum) p 117
Seeger K 1982 *Semiconductor Physics* (Berlin: Springer)
[49] Lei X L 2008 *Balance Equation Approach to Electron Transport in Semiconductors* (Singapore: World Scientific)
[50] Jiang J H and Wu M W 2009 *Phys. Rev.* B **79** 125206
Jiang J H and Wu M W 2011 *Phys. Rev.* B **83** 239906
[51] Zhang P, Zhou J and Wu M W 2008 *Phys. Rev.* B **77** 235323
[52] Tong H and Wu M W 2012 *Phys. Rev.* B **85** 075203
[53] Madelung O, Schultz M and Weiss H (ed) 1982 *Numerical Data and Functional Relationships in Science and Technology* (*Landolt-Börnstein, New Series, Group III* vol 17 Pt A) (Berlin: Springer)
[54] Shen K 2009 *Chin. Phys. Lett.* **26** 067201
[55] Krauß M, Schneider H C, Bratschitsch R, Chen Z and Cundiff S T 2010 *Phys. Rev.* B **81** 035213
[56] Tombros N, Tanabe S, Veligura A, Józsa C, Popinciuc M, Jonkman H T and van Wees B J 2008 *Phys. Rev. Lett.* **101** 046601
[57] Awschalom D D, Loss D and Samarth N (ed) 2002 *Semiconductor Spintronics and Quantum Computation* (Berlin: Springer)
[58] Gupta J A, Knobel R, Samarth N and Awschalom D D 2001 *Science* **292** 2458
[59] Wolf S A, Awschalom D D, Buhrman R A, Daughton J M, von Molnár S, Roukes M L, Chtchelkanova A Y and Treger D M 2001 *Science* **294** 1488
[60] Korn T 2010 *Phys. Rep.* **494** 415
[61] Cheng J L, Wu M W and Fabian J 2010 *Phys. Rev. Lett.* **104** 016601
[62] Li P and Dery H 2011 *Phys. Rev. Lett.* **107** 107203